This article has been accepted for publication in a future issue of this journal, but has not been fully edited. Content may change prior to final publication. Citation information: DOI 10.1109/TSTE.2019.2925089, IEEE Transactions on Sustainable Energy

Unbiased Circular Leakage Centered Adaptive Filtering Control for Power Quality Improvement of Wind-Solar PV Energy Conversion System

Farheen Chishti, *Member*, *IEEE*, Shadab Murshid, *Member*, *IEEE* and Bhim Singh, *Fellow*, *IEEE*

***Abstract*—The hybrid renewable energy conversion systems (HRECSs) and their increased penetration into the utility grid (UG) are intensifying the power quality (PQ) issues especially, in the form of increased total harmonic distortion (THD) of voltages and currents at point of common coupling (PCC). The objective of proposed grid tied wind-solar PV energy conversion system (ECS) is to analyze PQ issues and to mitigate them by utilizing the unbiased circular leakage centered (UCLC) adaptive filtering control. An implementation of UCLC adaptive control, improves the PQ indices and system performance by overcoming the intermittency issues associated with solar and wind energies. UCLC adaptive control effectively extracts the fundamental load current component and mitigates the grid current harmonics. It has simple structure, enhanced convergence rate and better performance with noise corrupted input and output signals. It effectively resolves the weight drift problem depicted by the conventional least mean square (LMS) control and leaky LMS control algorithm by avoiding biased estimates. The averaging theory and the deterministic stability analysis provide the relying facts of the performance of UCLC adaptive control. The extraction of maximum power from solar PV array energy and wind generation, is carried out by perturb and observe (P&O) scheme. A prototype is made in the laboratory and verified for environmental variations of solar insolation level, wind speed and perturbing load demand. The PQ issues are effectively alleviated. Test results confirm the effective performance of the proposed system.**

***Index Terms*—UCLC Adaptive Control, Load Compensation, Wind Energy Generation, Solar PV Generation, Utility Grid, and Power Quality.**

I. Introduction

THE glaring problem that the world, is facing today is the degradation of the environment due to escalating use of the fossil fuels and exploitation of the conventional natural resources, to meet the growing demand of energy. The awareness about environment and government initiatives, lead to the sense of conservation and rational utilization. The main aim at grass root level, is to challenge the structural designs and involved electro-mechanics in generation of power from the renewable resources [1]. The renewable resources such as, wind and solar are playing a major part in the global energy mix. They stand out to be inexhaustible, abundantly available, most promising resources for continually meeting the energy demand. They remain unaffected by the fluctuating oil prices and depletion of the fossil fuels. They righteously depend on the aberrant weather conditions [2]. The focus of the technocrats and the power providers, is to identify the period of highest load demand as well as highest electricity price and feed the highest generated power obtained by the renewables into the utility grid at that time. This acts as a source of additional revenue and can help in recovering the additional capital used for the installation of the system. The energy harnessed from the combinatorial use of the solar and wind, increases the system efficiency and power reliability. Each resource complements the other and thus reserve or storage requirements are cut-down [3-4]. Individually, they suffer from drawbacks of inherent intermittency and dependence on environmental conditions. However, the conjunction of two resources effectively provides energy and fulfills the load demand [5].

The utility connection to the microgrid involving wind and solar generation, widens its scope of operation. The assistance of the utility grid to the renewable operated system provides improved system operation, better customer service and ancillary benefits while improving reliability and resiliency. The demand response programs assist the customers/energy users to cut down the power usage at times when electricity price is high. The utility grid fulfills the load demand by assisting the insufficient generation obtained by the renewables as well as engrosses the excess generated power [6-7]. The grid connected wind-solar photovoltaic (PV) hybrid energy conversion system has been illustrated by the researchers describing effective methods for islanding and grid connected modes. Guo *et al.* [8] have investigated the co-generation from wind-solar PV energy conversion system (ECS) under grid associated and standalone modes. The grid associated ECS is capable to exchange power with the utility grid for power balance. Singh *et al.* [9] have analyzed hybrid renewable energy conversion system (HRECS) including wind, solar PV, battery and grid based on reliability for standalone and grid connected mode. Zhang *et al.* [10] have investigated the wind-solar microgrid from cost minimization view and addressed the unreliability of the HRECS.

The stochastic nature and the invariability associated with solar and wind energies, complicate the issue of smooth generation. The uncontrolled nature of HRECS can be controlled to some extend by utilizing advanced power electronic converters (PECs). However, the PECs inject harmonics owing to the intermittency associated with renewable power generation. Moreover, the power quality (PQ) is degraded due to power variability and unpredictability [11]. Chen *et al.* [12] have provided the review on the possible approaches of power electronic application in the wind energy generation system (WEGS). Two voltage source converters (VSCs) associated in back to back manner in between the utility grid and the wind generation unit, provide the variable revolutions per minute (RPM)-operation under variable wind speeds. The burden on the grid is highly reduced as well as the

This article has been accepted for publication in a future issue of this journal, but has not been fully edited. Content may change prior to final publication. Citation information: DOI 10.1109/TSTE.2019.2925089, IEEE Transactions on Sustainable Energy

resource utilization factor is maximized [13-14]. The asymmetric compensation is provided by the intermediate capacitor on both the VSCs as well as the decoupled control between the mechanical energy and the electrical energy.

Here, in the proposed work, the wind turbine drives the synchronous generator (SG). The wind turbine characteristics are imitated by the DC motor. The SG based WEGS harnesses the power from the unpredictable wind speed by using fully controlled VSC integrated with appropriate control scheme. The SG side converter (SGC) utilizes encoder-less field oriented control (FOC) [15-16] for generating proper switching signals. The SG rotor position and speed are required for FOC where the back electromotive force (BEMF) technique is implemented to serve the purpose. BEMF provides fast computation by eliminating complex observers. It is a significant speed estimation technique for high and medium speed assortments [17].

Solar PV array is connected across the DC link capacitor. The single stage topology utilizes reduced number of switches/components, which in turn cuts-down the related complexity issues and provides reduced cost and weight [18]. The power losses are reduced, simultaneously increasing the efficiency of the system [19]. Moreover, this configuration utilizes individual maximum power harnessing technique for solar PV and wind energies. For extraction of maximum power, extensive research and substantial literature have been reported in [20-23]. Here, perturb and observe (P&O) maximum power point (MPP) technique is used for extraction of optimal power from solar PV array and wind generation unit due to it simple structure and less computational burden on the processor.

The increased penetration of the renewables to the utility grid, poses intimidation to the PQ, load mismatch, frequency deviation and meager load following. Bubshait *et al.* [24] have presented a comprehensive control scheme for improving the power quality of the WEGS. The local load connected to the system, deteriorates the PQ and introduces grid current harmonics as it is nonlinear in nature. For PQ enhancement, numerous control schemes are reported in the literature for effectively switching the VSC connected to the grid [25-30]. The conventional control schemes addressing the PQ issues, are instantaneous power theory [25], conservative power theory (CPT) [26], synchronous reference frame theory (SRFT) [27] and improved linear sinusoidal tracer (ILST) [28]. Least mean squares (LMS) and its family of adaptive filtering techniques [29-30], prove to more efficient in conditions of external disturbances and changing environment.

LMS is based on the idea of minimizing the error by the use of stochastic gradient (Steepest Descent) method. Although it has very low computational burden, extra noise is introduced in the system estimates. The leaky LMS has increased computational burden when compared with LMS, whereas, the performance of the system remains intact under Eigen value spread. On comparing the performance of the two, the conclusion drawn is as follows.

- For any value of the leakage term, the stable range of perturbation step size for LMS is smaller than that of the leaky LMS with noisy inputs [31].
- For the stable values of step size and leakage term, the convergence of leaky LMS is faster than that of LMS with noisy inputs [31].
- The mean square error (MSE) of LMS is high during steady state than that for leaky LMS [31].
- The standard LMS technique has the limitation of unbounded weight estimates and poor steady state performance with the noisy signals [32]. To reduce the weight drift issue, leaky LMS is introduced in [33] but it has provided improved performance at the verge of introducing biased estimates.

Here, in this work, a novel application of the unbiased circular leakage centered (UCLC) adaptive filtering control is proposed for the control of utility grid side converter (UGC). It ensures the operative power flow to the nonlinear load and utility grid, with the aim of improving the PQ indices such as power factor (PF), total harmonic distortion (THD) and distortion PF (DPF) [34]. The UCLC adaptive filtering control incorporates the tap magnitude dependent leakage term, applied at each iteration only when it exceeds the prespecified limit (L_1). This results in reduced computational cost and cheaper implementation in comparison to leaky LMS and standard LMS. It provides load current fundamental component extraction, reactive power compensation and harmonics attenuation. Moreover, the fast system response at changing conditions, is achieved.

The contribution and significant features of proposed system, are given as follows.

- UCLC adaptive filtering control is proposed for addressing and mitigating the power quality issues.
- Fast response, easy implementation and harmonic elimination, are traits of UCLC adaptive filtering control.
- The unbounded rise of estimated weights with the bias issues, is effectively handled by UCLC adaptive control and performance comparison is shown in Table-I.
- The dynamics of the proposed system, are significantly improved by introducing the solar PV and wind feed-forward terms in the control scheme.
- Appropriate power generation with proper switching controls for UGC and SGC is obtained.
- An incorporation of multiple operating conditions including wide range of wind speeds and solar insolation.
- Performance estimation and conformation of the system response by test results obtained under large number of operating scenarios result in satisfying the IEEE-519 standard, i.e. grid current THD is found within 5% and enhanced PQ is obtained [35].

II. System Configuration

Grid assisted wind solar PV ECS is demonstrated in Fig. 1. The WEGS consists of SG driven by the wind turbine. The DC

TABLE-I
COMPARISON OF THE ADAPTIVE ALGORITHMS

Algorithm	Drift Problem	Biased Weights
Standard LMS	Yes	No
Leaky LMS	No	Yes
UCLC adaptive Control	No	No

This article has been accepted for publication in a future issue of this journal, but has not been fully edited. Content may change prior to final publication. Citation information: DOI 10.1109/TSTE.2019.2925089, IEEE Transactions on Sustainable Energy

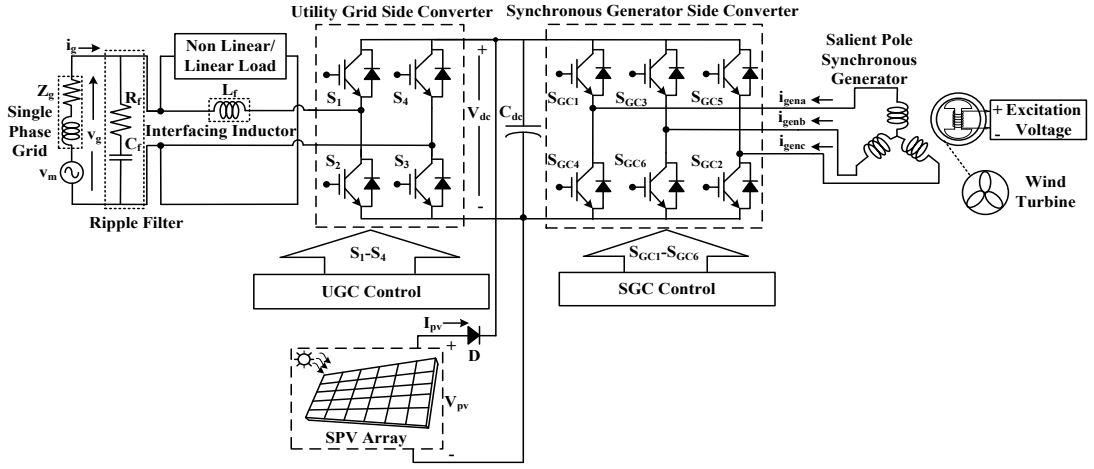

Fig.1 System Configuration.

link collects the energy from wind generation unit as well as from the single stage PV power generation array and then transfers the energy to feed the nonlinear load. To prevent the damage caused by the reverse flow of current, a blocking diode is associated in series of the solar PV array. The variable speed operation is realized by two back to back associated full rated VSCs. The SGC utilizes encoder-less FOC technique and estimated speed and rotor position are provided by BEMF scheme. The UGC utilizes UCLC adaptive filtering control technique for load compensation. The nonlinear load is realized by combining an uncontrolled rectifier with R-L load and is connected at the AC side of UGC. Switching harmonics are absorbed by the R-C ripple filter. Current harmonics and their effects are reduced by the interfacing inductor. The MPP is acquired individually from solar PV generation unit and wind power generation unit by utilizing P&O scheme named as, wind-P&O scheme and PV-P&O scheme, respectively. PV-P&O algorithm provides the reference DC link voltage and during the absence of solar generation, it is set to its default value. The system parameters, are given in Appendix.

III. Control Methodology

The proposed system utilizes effective control schemes for providing the switching pulses to SGC and UGC. The intermittency of renewable generation due to meteorological conditions, is undertaken. The adopted control schemes are elaborated in this section.

A. UCLC Adaptive Filtering Control for Switching UGC

Fig. 2 illustrates the switching control for the UGC. The UCLC control is utilized for estimating the fundamental component of the load current. It applies time variant leakage term in contrast to the fixed leaky term of leaky LMS. In doing so, unbiased weights are extracted, which avoid the unbounded rise of the weights.

1) Design of UCLC Adaptive Filtering Control

On the root level, the design criterion of the UCLC is based on the adaptive control schemes of the LMS family with improvements, which tend to remove drift issues and bias incurring in the weights.

The conventional LMS control gives weight update as,

$$w_{n+1}=w_n+\xi u_n e(n) \tag{1}$$

where, w_n is the estimated weight, u_n is the input, e(n) is the estimated error and ξ is the step size.

The leaky LMS introduced the leakage term to avoid unbounded growth of estimated weights and update is given as,

$$w_{n+1}=(1-\xi\delta_0)w_n+\xi u_n e(n) \tag{2}$$

where,$\xi\delta_0$ is the positive leakage term.

The weight update of UCLC adaptive filtering control is dependent on two conditions. First, the leakage is applied only when the magnitude of tap exceeds the prespecified limit (L_1).

$$\left|w^c_{n,\bar{n}}\right|>L_1 \tag{3}$$

where, $\bar{n}$=n mod M, and M is the individual entry of weight update vector ($w^c_{n,q}$) and q=1,2,3…M. Second, the leakage factor (δ_c) changes with time and is dependent on the tap magnitude. When (3) is satisfied, the intermediate weight vector is estimated as,

$$\bar{w}^c_n=\begin{bmatrix}\left\{\begin{matrix}w^c_{n,0}\\ \vdots\\ (1-\xi\delta_c(n,w^c_{n,\bar{n}}))w^c_{n,\bar{n}}\\ \vdots\\ w^c_{n,M-1}\end{matrix}\right\}, & \text{if } \left|w^c_{n,\bar{n}}\right|>L_1\\ w^c_n, & \text{otherwise}\end{bmatrix} \tag{4}$$

After, the intermediate estimate is computed, the UCLC adaptive filtering control update is given as,

$$w^c_{n+1}=(1-\xi\delta_c(n,w^c_{n,\bar{n}}))e_{\bar{n}}e^T_{\bar{n}})w^c_n+\xi u_n e^c(n) \tag{5}$$

The unbiased circular leakage term is given as,

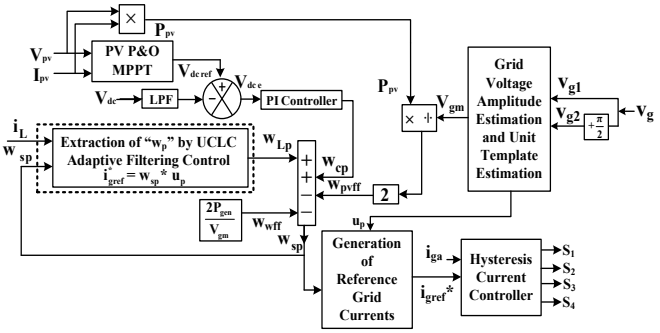

Fig. 2 Control Structure for UGC

This article has been accepted for publication in a future issue of this journal, but has not been fully edited. Content may change prior to final publication. Citation information: DOI 10.1109/TSTE.2019.2925089, IEEE Transactions on Sustainable Energy

$$\delta_c(n,w^c_{n,\bar{n}})=\begin{Bmatrix} \delta_o, \text{ if } |w^c_{n,\bar{n}}| \geq L_2 \\ \delta_0-\frac{\delta_0}{2}\left(\frac{L_2-|w^c_{n,\bar{n}}|}{D}\right)^2 \\ \text{if } L_1+D \leq |w^c_{n,\bar{n}}| < L_2 \\ \frac{\delta_0}{2}\left(\frac{|w^c_{n,\bar{n}}|-L_1}{D}\right)^2 \\ \text{if } L_1 < |w^c_{n,\bar{n}}| < L_1+D \\ 0, \quad \text{Otherwise} \end{Bmatrix} \quad (6)$$

where, L_1 is the prespecified limit, $L_2 > L_1$ are positive constants, and $D=(L_2-L_1)/2$.

A simple method of implementing the unbiased circular leakage term with hard-limiting is also valid and is given as,

$$\delta_c(a)=\begin{Bmatrix} \delta_0, \text{ if } |a|>L_1 \\ 0, \text{ if } |a| \leq L_1 \end{Bmatrix} \quad (7)$$

Table-II depicts the leakage term and its applicability according to the adaptive control algorithms.

The drift problem of LMS is illustrated by the time invariant linear equation given as [32],

$$w_n=\frac{10^{-4}}{n}\sum_{i=1}^{n}\sqrt{i} \geq \frac{2*10^{-4}}{3}\sqrt{n} \quad (8)$$

When $n\rightarrow\infty$, then $w_n\rightarrow\infty$. This gives the information that the estimated weights rise to large values even when the noise is low. As a solution to the drift problem, leakage term disallowed the unbounded rise of the estimated weights. The recursion equation is given as [33],

$$w_{n+1}=\left(1-\xi\delta_0-\frac{\xi}{n+1}\right)w_n+\xi\delta_0 w_*-\xi\frac{10^{-4}}{\sqrt{n+1}} \quad (9)$$

This results in a bounded sequence given as,

$$\{w_n\} \text{ if } 0<\xi<2/(\delta_0+1) \quad (10)$$

As an outcome, bias problem arises in leaky LMS and is specified by means of,

$$w_{n+1}=((1-\xi\delta_0)I-\xi u_n u_n^T)w_n+\xi\delta_0 w_*-\xi u_n v_n \quad (11)$$

where, u_n and v_n are independent and stationary sequences. Evaluating the expectation (E) of w_{n+1} as,

$$Ew_{n+1}=((1-\xi\delta_0)I-\xi R)Ew_n+\xi\delta_0 w_* \quad (12)$$

where, R=Regressor covariance matrix $=Eu_nu_n^T$. The steady state equation is given as,

$$\lim_{n\rightarrow\infty} Ew_n=\delta_0(\delta_0 I+R)^{-1}w_* \quad (13)$$

The evaluated weights do not converge to zero even when there is no error and no noise. Alternate solution for the bias problem is a very small leakage value, but it is unable to counter the effects of finite precision arithmetic.

TABLE-II

APPLICATION OF LEAKAGE IN ADAPTIVE ALGORITHMS

Algorithm	Condition to Apply Leakage	Leakage Term
Standard LMS	Not applicable	Not applicable
Leaky LMS	Always applied on all taps	$\xi\delta_0 w_n$
UCLC adaptive Control	Applied on single tap when $\|w^c_{n,\bar{n}}\|>L_1$	$\xi\delta_c(n,w^c_{n,\bar{n}})e_{\bar{n}}e_{\bar{n}}^T w^c_n$

The UCLC adaptive filtering algorithm establishes its stochastic performance based on the averaging analysis and deterministic performance based on Lyapunov stability.

The recursion equation is given as,

$$w^c_{n+1}=(I-\xi\delta_c(w_{k,\bar{k}})e_{\bar{k}}e_k^T-\xi u_n u_n^T)w^c_n+\xi\delta_c(w_{k,\bar{k}})e_{\bar{k}}e_k^T w_*-\xi u_n v_n-\alpha^c_n \quad (14)$$

On averaging (14) over u_n and noise v_n and finite precision error α_n^c, the equation obtained is given as,

$$w^c_{n+1}=(I-\xi\delta_c(w_{*,\bar{k}}-w_{k,\bar{k}})e_{\bar{k}}e_k^T-\xi R)w^c_n+\xi\delta_c(w_{*,\bar{k}}-w_{k,\bar{k}})e_{\bar{k}}e_k^T w_* \quad (15)$$

The condition (15) is satisfied for values of ξ and δ_0 as,

$$\xi(1+\frac{1}{\tau_c})\delta_0<2-\xi\gamma_{max}(R) \quad (16)$$

where, τ_c is a constant > 0 and fulfills the condition,

$$L_1 \geq (1+\tau_c)\|w_*\|_\infty \quad (17)$$

If ξ is small, then unbiased circular leakage in steady state is given as,

$$\lim_{n\rightarrow\infty} Ee^c(n)^2 \approx \beta_v^2+\xi(\beta_v^2+\beta_d^2).\frac{Tr(R)}{2}+\frac{Tr(\beta_d^2(I+R)}{2} \quad (18)$$

where, the variance is given by β, $E\eta(n)=\beta_v$ and $E\xi_n^2=\beta_d^2$.

The stability of the UCLC adaptive filtering algorithm is satisfied when the condition given is fulfilled.

$$|1-\xi\delta_0-\xi\psi|<1 \quad (19)$$

$$\sqrt{1-\frac{\xi\delta_0(2-\xi\delta_0)}{M}}+\xi M\psi<1 \quad (20)$$

where, ψ is the bounded region and the UCLC control exhibits bounded input and bounded state stability by (19) and (20).

2) Unit Template Estimation

The sensed voltage from the PCC is used to estimate the amplitude of peak grid voltage (v_g) and is given as,

$$V_{gm}=\sqrt{v_{g1}^{\ 2}+v_{g2}^{\ 2}} \quad (21)$$

where, v_{g1} is the in-phase fundamental component of v_g and v_{g2} is the quadrature phase fundamental component of v_g.

The unit template is evaluated using calculated peak grid voltage and v_{g1} as,

$$u_p=\frac{v_{g1}}{V_{gm}} \quad (22)$$

3) Assessment of Fundamental Load Current Component

The weight of the fundamental load current component is calculated using the UCLC adaptive filtering algorithm and is given as,

$$w^c_{Lp\,n+1}=(1-\xi\delta_c(n,w^c_{Lp\,n,\bar{n}}))e_{\bar{n}}e_{\bar{n}}^T)w^c_{Lp\,n}+\xi u_p e^c(n) \quad (23)$$

The error is given as,

$$e^c(n)=i_L(n)-u_p^T w^c_{Lp\,n}(n) \quad (24)$$

The DC error component ($V_{dc\,e}$) is estimated by equating the reference DC link voltage to V_{dc}. The proportional integral (PI) controller is used to regulate the DC link voltage at the MPP voltage of the solar PV array. Dispensing of the steady state error is done by the integral part and it is very weak.

The output equation of the PI controller is given as,

$$w_{cp}(n)=w_{cp}(n-1)+k_i\{V_{dc\,e}(n)-V_{dc\,e}(n-1)\}+k_p V_{dc\,e}(n) \quad (25)$$

The feed-forward terms of wind (w_{wff}) and solar PV array (w_{pvff}) enhance the dynamic performance of proposed ECS and they are evaluated as,

This article has been accepted for publication in a future issue of this journal, but has not been fully edited. Content may change prior to final publication. Citation information: DOI 10.1109/TSTE.2019.2925089, IEEE Transactions on Sustainable Energy

$$w_{wff}=\frac{2P_{gen}}{V_{gm}} \quad (26)$$

$$w_{pvff}=\frac{2P_{PV}}{V_{gm}} \quad (27)$$

where, P_{gen} and P_{pv} denote power generated from wind generation unit and solar PV array, respectively. The feed-forward terms allow to determine the total active current injection into the utility grid.

4) Reference Current Assessment and Switching Control for the UGC

The net grid active power component (w_{sp}) is calculated as,

$$w_{sp}=w_{cp}+w_{Lp}-w_{PVff}-w_{wff} \quad (28)$$

The grid reference current ($i_{g\,ref}$*) is estimated by the product of net grid current amplitude with u_p and is evaluated as,

$$i_{g\,ref}^{*}=w_{sp}\times u_p \quad (29)$$

The sensed grid current and $i_{g\,ref}$* are compared, and the difference is fed to the hysteresis current controller (HCC). The switching pulses (S_1 to S_4) are provided as the output of the HCC to UGC.

B. Encoder-Less Switching Control of SGC

Fig. 3 represents the switching control logic of SGC. The FOC provides the excellent generator speed control. The speed and position are estimated by using the encoder-less BEMF technique. The organization of BEMF scheme is derived from [36-37]. The FOC of the AC machine emulates the DC machine control by giving correct orientation together in steady state and dynamic conditions. The FOC resolves the three phase stator currents in the stationary reference frame into field and torque producing components by coordinate transformation (3phase to d-q axis) providing linear relationship between control variables and torque. FOC provides decoupled and independent control of flux and the torque components. The control of field current and the torque, controls the flux and torque components. The switching control of SGC regulates the generation from the direct axis reference current ($I_{d\,ref}$) and quadrature axis reference current ($I_{q\,ref}$).

1) Assessment of Quadrature Axis Reference Current Component ($I_{q\,ref}$)

Wind P&O MPP algorithm determines the reference SG speed ($\omega_{gen\,ref}$). An optimal power point is traced by perturbing the speed (ω_{gen}) and power (P_{gen}) of the wind turbine driven SG.

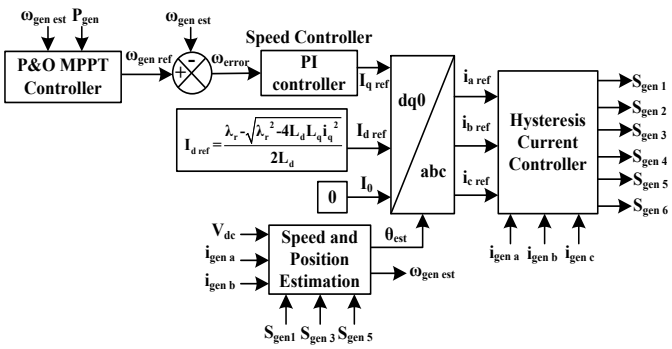

Fig. 3 Control Structure for SGC

The dominating equation of wind P&O scheme is given as,

$$\omega_{gen\,ref}(n)=\omega_{gen\,ref}(n\text{-}1)+\Delta\omega_{gen};\ \text{if}\begin{Bmatrix}\Delta P_{gen}>0 \text{ and } \Delta\omega_{gen\,est}>0\\ \Delta P_{gen}<0 \text{ and } \Delta\omega_{gen\,est}<0\end{Bmatrix} \quad (30)$$

$$\omega_{gen\,ref}(n)=\omega_{gen\,ref}(n\text{-}1)-\Delta\omega_{gen};\ \text{if}\begin{Bmatrix}\Delta P_{gen}>0 \text{ and } \Delta\omega_{gen\,est}<0\\ \Delta P_{gen}<0 \text{ and } \Delta\omega_{gen\,est}>0\end{Bmatrix} \quad (31)$$

The speed error (ω_{error}) of SG is calculated by equating $\omega_{gen\,ref}$ with the estimated SG speed ($\omega_{gen\ est}$) and the governing equation is given as,

$$\omega_{error}(n)=\omega_{gen\,ref}(n)-\omega_{gen\,est}(n) \quad (32)$$

The PI speed controller takes ω_{error} as the input and gives $I_{q\,ref}$ as the output, which is given as,

$$I_{q\,ref}(n)=I_{q\,ref}(n\text{-}1)+k_{igen}\{\omega_{error}(n)-\omega_{error}(n\text{-}1)\}+k_{pgen}\{\omega_{error}(n)\} \quad (33)$$

where, the speed PI controller proportional and integral gains are given as k_{pgen} and k_{igen} respectively.

2) Assessment of Direct Axis Reference Current Component ($I_{d\,ref}$)

The unity power factor (UPF) is sustained by the SG stator terminals by controlling the direct axis reference current component and enabling the stator power factor angle (θ_s) to zero value. The governing equation of calculating $I_{d\,ref}$ is specified as,

$$I_{d\,ref}=\frac{\lambda_r-\sqrt{\lambda_r^{\,2}-4L_dL_qI_q^{\,2}}}{2L_d} \quad (34)$$

where, λ_r is the rotor flux linkage, L_d is the d-axis inductance and L_q is the q-axis inductance.

3) Switching Signal Generation for SGC

The SG stator reference currents ($i_{a\,ref}$, $i_{b\,ref}$, $i_{c\,ref}$) are generated by $I_{d\,ref}$ and $I_{q\,ref}$ undergoing the inverse Park's transform (dq0 to abc). The HCC compares the sensed SG stator currents (i_{gena}, i_{genb}, i_{genc}) and reference stator currents and generate the switching signals ($S_{gen\,1}$ to $S_{gen\,6}$) for SGC.

IV. Results and Discussion

The performance of the wind-solar PV energy conversion system is studied experimentally on the developed laboratory prototype. To sense the PCC voltages, solar PV array voltage, DC link voltage, Hall-Effect based voltage sensors (LEM-LV25-P) are used. To sense the load currents, SG currents, grid current, solar PV array current, Hall-Effect based current sensors (LEM-LA55-P) are used. The opto-couplers provide adequate insolation in between the switching signals and the voltage source converter. The solar PV generation characteristic is realized using solar PV simulator (AMETEK-ETS600x17DPVF).

The control algorithms are implemented using the digital signal processor (Dspace-1202 Microlab-box). The steady state response of the system is recorded by power analyzer (Fluke-43B). Two back to back associated converters (SEMIKRON make) are utilized for decoupled control of mechanical and electrical power. The wind turbine characteristics are obtained by the DC machine (BENLEC make) imitated as the wind turbine. The SG (BENLEC make) is coupled to the DC machine. Experimental parameters utilized for the substantiation of the proposed ECS, are provided in Appendix.

This article has been accepted for publication in a future issue of this journal, but has not been fully edited. Content may change prior to final publication. Citation information: DOI 10.1109/TSTE.2019.2925089, IEEE Transactions on Sustainable Energy

Test results are discussed in following sections.

A. Performance of System under Steady State

Fig. 4 illustrates the performance of the system when wind and solar are unable to supply active power due to low solar intensity and low wind speeds. The UGC transits to the distribution static compensator (DSTATCOM) mode. The proposed system works in coordination with the amalgamation of the DSTATCOM capabilities to alleviate PQ concerns with smarter feasible approach for the periods when the generation from the HRECSs is not available.

The proposed approach provides 24 hour operational assessment of energy from HRECSs with DSTATCOM functionality. The issue of addressing the stochastic behavioral generation from hybrid wind and solar PV array has been addressed. This brings into light many of the concerns regarding lifetime consumption assessment and functionality of different modes of operation. During night hours/foggy/hazy atmosphere, the generation from solar PV array is not sufficient due to insufficient insolation level. Therefore the UGC acts in the DSTATCOM mode enabling, reactive power compensation and harmonics elimination. The reactive power required by the nonlinear load, is fully compensated by the DSTATCOM mode of operation. The utility grid does not supply any of the reactive power in this mode of operation. The anticipated approach considered in this work is capable of working in low solar insolation level and low wind speeds, providing enhanced system operation.

Fig. 4(a) shows the response of gird voltage, grid current, UGC current in DSTATCOM mode and load current. The grid current is found sinusoidal under DSTATCOM operating mode. Fig. 4 (b) shows the response of the system when the PV array and wind generating units, are working on their full rated capacity. The grid current magnitude is increased and UGC current has an increased magnitude with its waveform being less distorted. The load current remains constant.

Fig. 5 depicts the voltage and current waveform of the grid with the power of the grid that is being fed to the load. The THD of the grid current is found 4.2% and the grid voltage THD is found 3.3%, i.e. confirming the limits of the IEEE-519 standard. The load voltage and current waveforms with the load power that is being consumed by the load from the grid, are depicted in Fig. 6. The THD of the load current is found 22.7% and the load voltage THD is found 3.7%, i.e. well within the limits of the IEEE-519 standard. The waveform and magnitude of the current, voltage and power of the UGC are illustrated in Fig. 7. The THD of the UGC current is found 72.0 % and UGC voltage THD is found 3.8%.

Fig. 8 depicts the grid voltage and current waveforms with the grid power that is being fed to the grid by the wind and PV power. The surplus power is fed to the grid. The THD of the grid current is found 2.3% and the grid voltage THD is found 2.8 %, i.e. well within the limits of the IEEE-519 standard. Fig. 9 depicts the waveforms and magnitude of the voltage, current and power that is being consumed by the load. The THD of the load current is found 22.6% and the load voltage THD is found 3.1%, i.e. well within the limits of the IEEE-519 standard. Fig. 10 demonstrates the waveforms and magnitude of the current, voltage and power of the UGC. The THD of the UGC current is found 6.8 %.

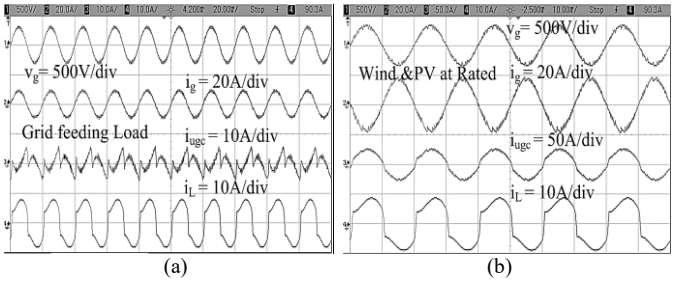

(a) (b)

Fig. 4 Performance of proposed ECS at steady state.

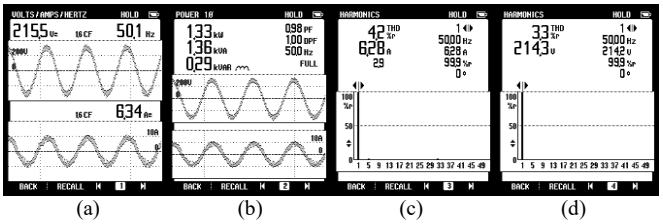

(a) (b) (c) (d)

Fig. 5 Response of (a) v_g and i_g, (b) grid power, (c) grid current THD, (d) grid voltage THD when grid is feeding load.

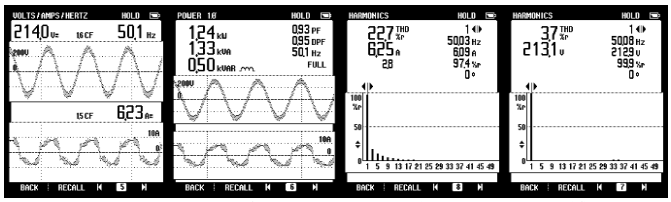

(a) (b) (c) (d)

Fig. 6 Response of (a) v_l and i_l, (b) load power, (c) load current THD, (d) load voltage THD when grid is feeding load.

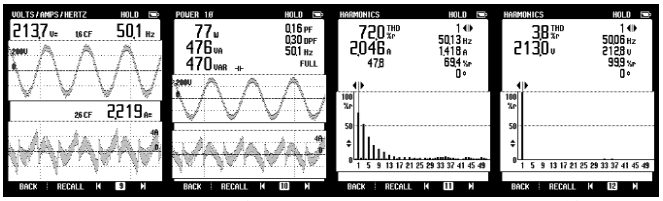

(a) (b) (c) (d)

Fig. 7 Response of (a) UGC voltage and current waveform, (b) UGC power, (c) UGC current THD, (d) UGC voltage THD when grid is feeding the load.

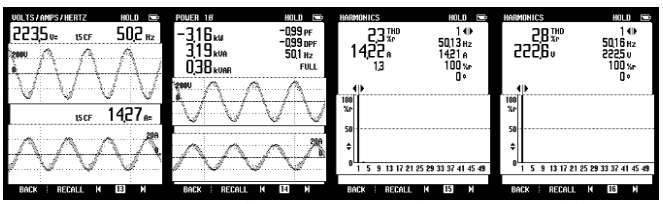

(a) (b) (c) (d)

Fig. 8 Response of (a) v_g and i_g, (b) grid power, (c) grid current THD, (d) grid voltage THD under wind and PV at rated condition.

B. Dynamic Performance of System at Varying Wind Velocity

Fig. 11 depicts performance of the system under variable wind speeds. The wind speed should neither be above the cut-out wind speed, nor below the cut-in speed. However, the wind speed other than specified wind speed range does not provide useful power. Fig. 11 (a) shows that, when the change (i.e. 12m/s to 7.2m/s) in wind speed (v_{wind}) takes place, the estimated generator speed ($\omega_{gen\ est}$) decreases and simultaneous decrease in the direct axis current (I_d) and quadrature axis current (I_q) can be seen and vice versa. Fig. 11 (b) presents the scenario when there is an increase in wind speed, $\omega_{gen\ est}$ increases while increasing the generator currents (i_{gen}) and the estimated rotor position (θ_{est}) keeping the DC link voltage at the MPP voltage

This article has been accepted for publication in a future issue of this journal, but has not been fully edited. Content may change prior to final publication. Citation information: DOI 10.1109/TSTE.2019.2925089, IEEE Transactions on Sustainable Energy

of the solar PV array. Fig. 11 (c) presents the change due to an increase in wind speed and the simultaneous increase in generator currents (i_{gen}), grid current (i_g) and the UGC current (i_{ugc}) while maintaining the load current (i_L) constant.

C. Dynamic Performance at Varying Solar Insolation Level

Fig. 12 depicts the performance of the system under changing level of solar insolation. It is shown in Figs. 12 (a)-(b) that, when the solar insolation is decreased, the PV current (I_{pv}) decreases as well as the PV power (P_{pv}) decreases, reducing the power level that is fed into the grid and vice versa. The DC link voltage (V_{dc}) is same as the PV array voltage (V_{pv}) and it is adjusted in accordance with PV MPP controller. Figs. 12 (c)-(d) show the grid current (i_g), UGC current (i_{ugc}) and load current (i_L) performance along with I_{pv}, when the solar insolation rises and falls. When the level of solar insolation decreases, the PV current reduces, the grid current reduces as the power fed into the grid is reduced and simultaneously the UGC current reduces while keeping the load current constant and vice versa. It justifies that the load demand is always fulfilled by the proposed system.

D. Dynamic Performance at Load Perturbation

Fig. 13 demonstrates the response of proposed ECS at load

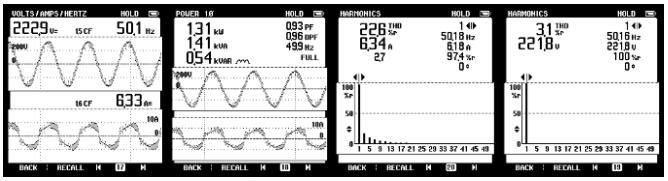

(a) (b) (c) (d)

Fig. 9 Response of (a) v_l and i_l,, (b) load power, (c) load current THD, (d) load voltage THD under wind and PV at rated condition.

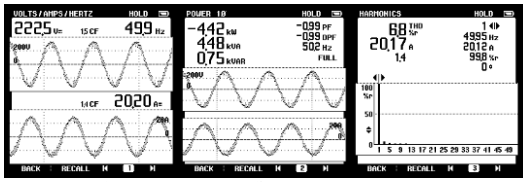

(a) (b) (c)

Fig. 10 Waveforms of (a) UGC voltage and current waveform, (b) UGC power, (c) UGC current THD, (d) UGC voltage THD under wind and PV at rated condition.

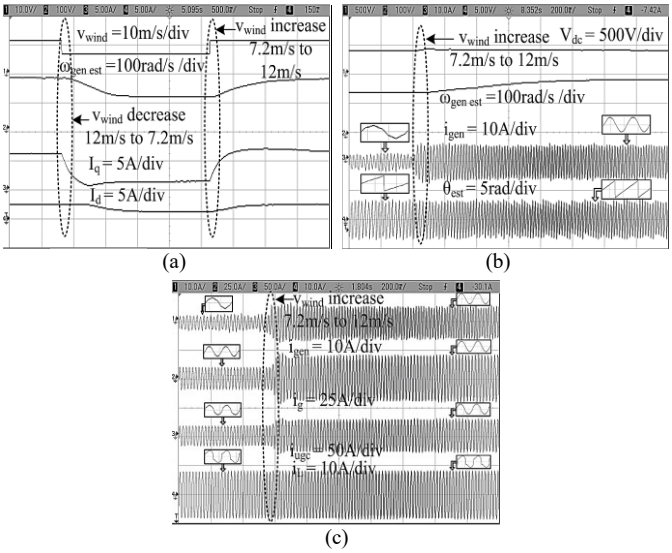

(a) (b) (c)

Fig. 11 Dynamic performance of proposed system under varying wind speed.

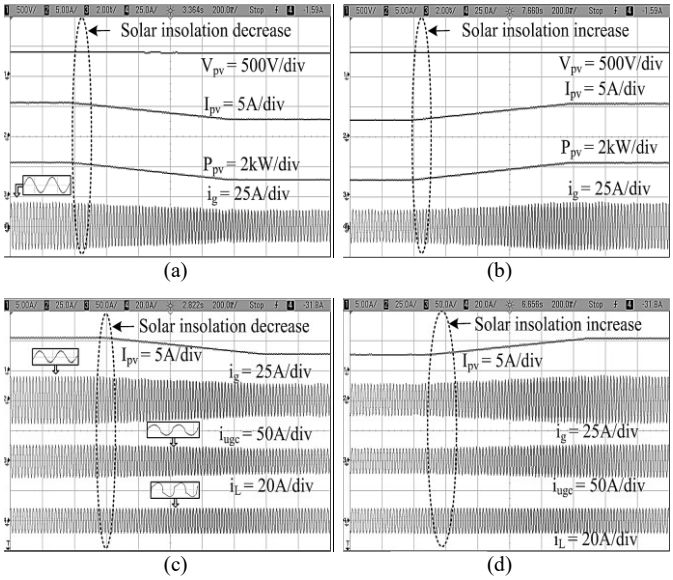

(a) (b) (c) (d)

Fig. 12 Response of proposed ECS at varying solar insolation level.

perturbation, which includes load addition, load reduction, load removal (throw) and load inclusion. Fig. 13 (a) shows the response under load reduction. V_{dc} is maintained at the MPP voltage of the solar PV array and v_L remains constant whereas due to reduction in load, the load current (i_L) decreases and the grid current (i_g) increases. Fig. 13 (b) shows the contrary condition of load addition. As the load is increased the load current increases and the grid current decreases.

Figs 13 (c)-(d) depict the condition of load thrown and load inclusion. When the load is removed completely, the load current is zero. The power consumed by the load is fed to the grid and as a result, the grid current increases and vice versa. Fig. 13 (e) demonstrates the condition for the load reduction in which the load current decreases gradually, increasing the grid current and simultaneously increasing the UGC current, whereas, the PV current is maintained constant.

Fig. 13 (f) shows the contrary scenario of load addition, in which, when the load is added, the grid current decreases, the load current increases and the UGC current decreases. On the other hand, disconnection of load from the system, leads to zero load current, increased grid current and UGC current while maintaining the PV current constant and vice versa. The response can be clearly seen from Figs. 13 (g)-(h). In the case, when the load is reduced, the load current gradually decreases, while decreasing the fundamental current (i_{fund}) generated and maintaining the unit template constant in magnitude. Figs. 13 (i)-(j) show the illustrated condition and the contrary condition.

E. Solar MPP Performance

Fig. 14 (a) represents the tracking of the solar maximum power point performance under maximum solar insolation level i.e. 1000W/m^2. The optimal power harvested from the solar PV array is 2.34 kW. The MPP achieved is 99.55%. Fig. 14 (b) depicts the maximum power extracted from the solar PV array at 500w/m^2 solar insolation. The power extracted is about 1.17kW at 99.71% MPP.

G. Comparative Analysis of UCLC Adaptive Control

The enhanced performance of the UCLC adaptive control is presented in Table - III. The UCLC is compared with other

This article has been accepted for publication in a future issue of this journal, but has not been fully edited. Content may change prior to final publication. Citation information: DOI 10.1109/TSTE.2019.2925089, IEEE Transactions on Sustainable Energy

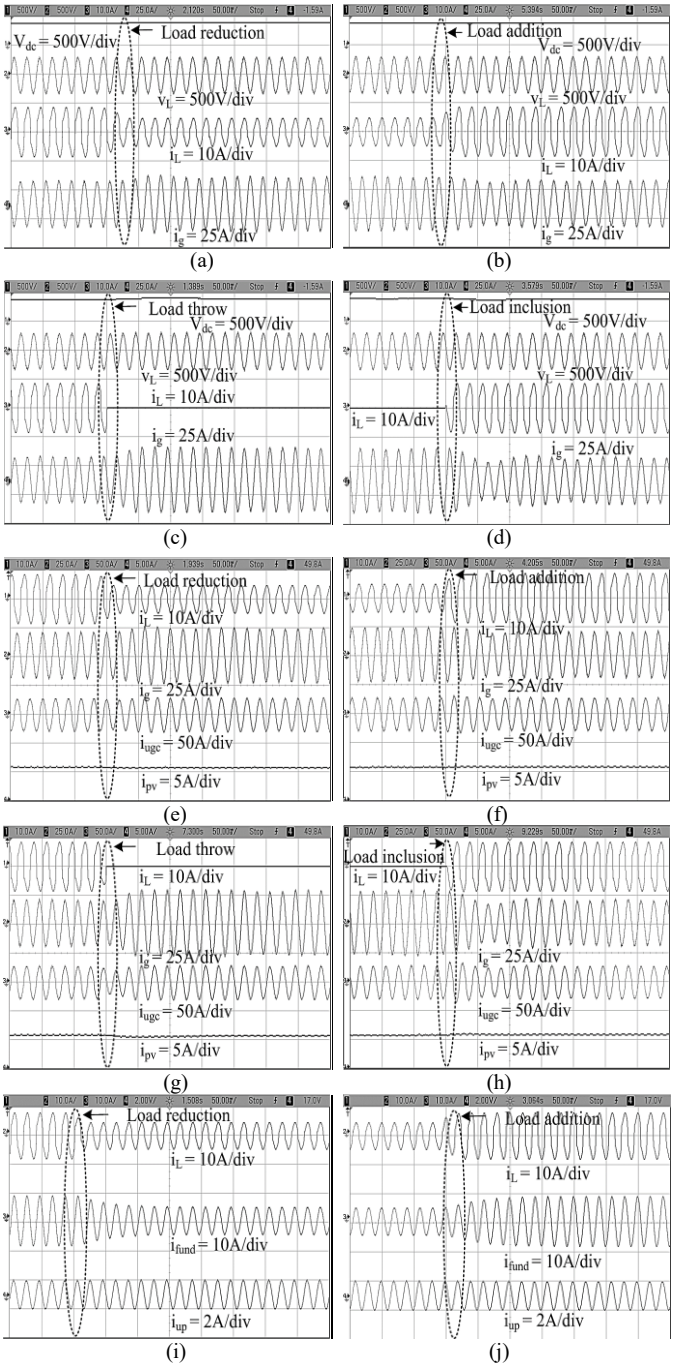

Fig. 13 Performance of proposed ECS under load perturbation.

adaptive control and proves to be more effective in functioning. Fig. 15 illustrates the relative response of UCLC with conventional adaptive algorithm i.e. leaky LMS. Fig. 15 (a) shows that the convergence rate of leaky LMS algorithm is relatively slower, with higher level of oscillations in the active weight component during load disconnection. This leads to slow reference current component generation. The response of the control is shown for load reconnection in Fig. 15 (b). It is observed that, the control has higher level of jittering during reconnection. It takes time to settle to a stable value. The performance of the UCLC adaptive filtering control is observed in Figs. 15 (c-d). UCLC outperforms the conventional adaptive algorithm and provides faster convergence rate with reduced ripples in the active weight component during disconnection of

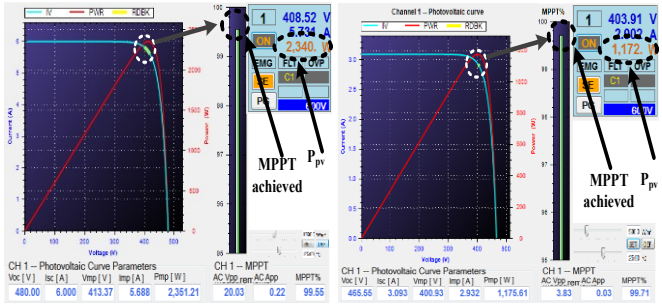

Fig. 14. Solar PV array MPP performance.

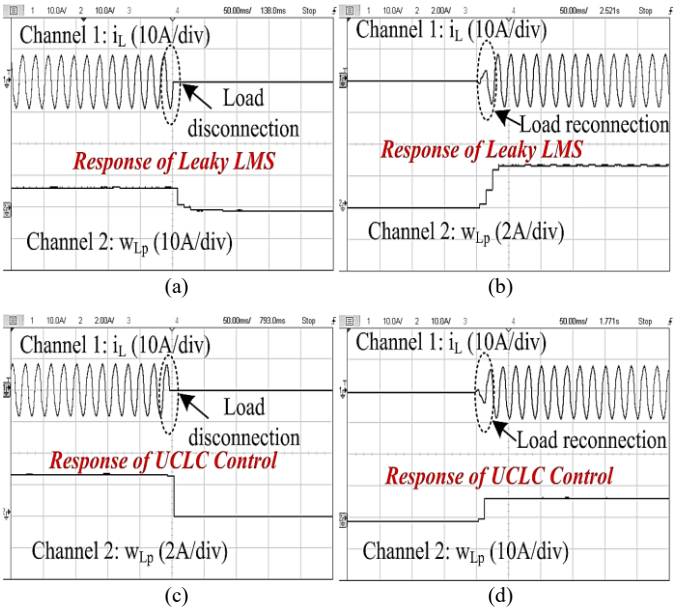

Fig. 15 Comparative performance of UCLC adaptive filtering control with the conventional control algorithm.

TABLE-III

COMPARATIVE ANALYSIS OF ADAPTIVE ALGORITHMS

Algorithm	Static Error	Accuracy	Tracking Speed	Settling Time	V_{dc} Oscillations
LMS	More	Poor	Moderate	More	Medium
Leaky LMS	Low	Good	Fast	Less	Low
UCLC	Low	Better	Fast	Low	Very Low

load and reconnection. The better performance of UCLC with respect to leaky LMS is confirmed.

V. CONCLUSION

The UCLC adaptive filtering control for wind-solar PV energy conversion system has been implemented successfully on a laboratory prototype to demonstrate its performance in accordance to the dynamic wind speed conditions, varying solar insolation level and altering load demand. The concluding remarks are summarized as follows.

- UCLC adaptive filtering scheme has successfully mitigated the grid current harmonics and enhanced power quality is attained at the input AC mains.
- UCLC has effectively estimated the sinusoidal fundamental active load current component by filtering the disturbances and harmonics component.
- It has provided improved filtering response in both steady

state and dynamic conditions.

- It has proved to be simple in organization easy to implement and responds fast as it is less computationally exhaustive during its execution.
- An improved proficiency of the control technique has been observed by successful extraction of fundamental load active component.
- Enhanced dynamic response and flexible system operation have been attained by including solar and wind feed-forward terms.
- The PQ enhancement is validated in accordance to the IEEE-519 standard, maintaining the grid current THD with the acceptable range i.e. below 5%.
- The solar and wind MPPTs show good steady state and dynamic performances on different insolation and wind speeds.

Test results manifest that the obtained response is satisfactory and acceptable. The computational burden offered by the control, is low and tracking time is very less.

ACKNOWLEDGEMENT

The authors are thankful to J. C. Bose project (Grant Number: RP03128), Grant Number: RP03391 (UKICERI) and Grant Number: RP-03357 (CLEAN ENERGY DST) for financially supporting this work.

APPENDIX

A. SG Parameters: 415V, 5hp, Rs = 3.1Ω, Poles = 4, field excitation voltage: 220 V.
B. Solar PV array: 2.4 kW.
C. DC Motor: 220V, 19A, 5hp.
D. Wind Speed Range: cut-in (7.2m/s) to cut-out (12m/s).
E. DC Link Voltage: Vdc: 400V.
F. Parameters of Ripple Filter: $C_f = 10\ \mu F$, $R_f = 5\Omega$.
G. PI Controller Gains: $k_p = 1.2$; $k_i = 0.0001$.
H. UCLC Adaptive Filter Parameters: $\xi = 0.0001$; $L_1 = 0.8$, $L_2 = 0.81$, $\delta_0 = 0.1$.
I. Single Phase Nonlinear Load = 1.31kW.

REFERENCES

[1] P. Mallet, P. Granstrom, P. Hallberg, G. Lorenz and P. Mandatova, "Power to the people!: european perspectives on the future of electric distribution," *IEEE Pow. Ener. Mag.*, vol. 12, no. 2, pp. 51-64, March-April 2014.

[2] J. Varela, N. Hatziargyriou, L. J. Puglisi, M. Rossi, A. Abart and B. Bletterie, "The igreengrid project: increasing hosting capacity in distribution grids," *IEEE Pow. Ener. Mag.*, vol. 15, no. 3, pp. 30-40, May-June 2017.

[3] Y. Zhang, N. Gatsis and G. B. Giannakis, "Robust energy management for microgrids with high-penetration renewables," *IEEE Trans. Sustain. Energy*, vol. 4, no. 4, pp. 944-953, Oct. 2013.

[4] A. Merabet, K. Tawfique Ahmed, H. Ibrahim, R. Beguenane and A. M. Y. M. Ghias, "Energy management and control system for laboratory scale microgrid based Wind-PV-Battery," *IEEE Trans. Sustain. Energy*, vol. 8, no. 1, pp. 145-154, Jan. 2017.

[5] Y. Li, L. Fan and Z. Miao, "Stability control for wind in weak grids," *IEEE Trans. Sustain. Energy*, Early Access, 2019.

[6] X. Huang, K. Wang, B. Fan, Q. Yang, G. Li, D. Xie and M. L. Crow, "Robust current control of grid-tied inverters for renewable energy integration under non-ideal grid conditions," *IEEE Trans. Sustain. Energy*, Early Access, 2019.

[7] M. M. Amin and O. A. Mohammed, "Development of high-performance grid-connected wind energy conversion system for optimum utilization of variable speed wind turbines," *IEEE Trans. Sustain. Energy*, vol. 2, no. 3, pp. 235-245, July 2011.

[8] Y. Guo and C. Zhao, "Islanding-aware robust energy management for microgrids," *IEEE Trans. Smart Grid*, vol. 9, no. 2, pp. 1301-1309, March 2018.

[9] R. Singh, R. C. Bansal, A. R. Singh and R. Naidoo, "Multi-objective optimization of hybrid renewable energy system using reformed electric system cascade analysis for islanding and grid connected modes of operation," *IEEE Access*, vol. 6, pp. 47332-47354, 2018.

[10] C. Zhang, Y. Xu, Z. Y. Dong and J. Ma, "Robust operation of microgrids via two-stage coordinated energy storage and direct load control," *IEEE Trans. Pow. Sys.*, vol. 32, no. 4, pp. 2858-2868, July 2017.

[11] J. Xu, Q. Qian, B. Zhang and S. Xie, "Harmonics and stability analysis of single-phase grid-connected inverters in distributed power generation systems considering phase-locked loop impact," *IEEE Trans. Sustain. Energy*, Early Access, 2019.

[12] Z. Chen, J. M. Guerrero and F. Blaabjerg, "A review of the state of the art of power electronics for wind turbines," *IEEE Trans. Pow. Elect.*, vol. 24, no. 8, pp. 1859-1875, Aug. 2009.

[13] F. Blaabjerg and K. Ma, "Future on power electronics for wind turbine systems," *IEEE Jour. Emerg. Sel. Top. Pow. Elect*, vol. 1, no. 3, pp. 139-152, Sept. 2013.

[14] A. Radwan and Y. Mohamed, "Grid-connected wind-solar cogeneration using back-to-back voltage source converters," *IEEE Trans. Sustain. Energy*, Early Access, 2019.

[15] J. W. Finch and D. Giaouris, "Controlled AC electrical drives," IEEE Trans. Ind. Elect., vol. 55, no. 2, pp. 481-491, Feb. 2008.

[16] F. Briz, M. W. Degner, P. Garcia and R. D. Lorenz, "Comparison of saliency-based sensorless control techniques for AC machines," IEEE Trans. Ind. Appl., vol. 40, no. 4, pp. 1107-1115, July-Aug. 2004.

[17] M. Tawadros, J. Rizk and M. Nagrial, "Estimation of commutation instances using back EMF mapping for sensorless control of brushless permanent magnet motors," *IET Elect. Pow. Appl.*, vol. 7, no. 4, pp. 270-277, 2013.

[18] U. Shipurkar, J. Dong, H. Polinder and J. A. Ferreira, "Availability of wind turbine converters with extreme modularity," *IEEE Trans. Sustain. Energy*, vol. 9, no. 4, pp. 1772-1782, Oct. 2018.

[19] T. Wu, C. Chang, L. Lin and C. Kuo, "Power loss comparison of single- and two-stage grid-connected photovoltaic systems," *IEEE Trans. Ener. Conv.*, vol. 26, no. 2, pp. 707-715, June 2011.

[20] M. Heydari and K. Smedley, "Comparison of maximum power point tracking methods for medium to high power wind energy systems," *Proc. 20th Conf. Elect. Pow. Dist. Netw. Conference*, pp. 184-189, 2015.

[21] Z. Chen, M. Yin, Y. Zou, K. Meng and Z. Dong, "Maximum wind energy extraction for variable speed wind turbines with slow dynamic behavior," *IEEE Trans. Pow. Sys.*, vol. 32, no. 4, pp. 3321-3322, July 2017.

[22] H. S. Sahu and S. K. Nayak, "Extraction of maximum power from a PV array under non uniform irradiation conditions," *IEEE Trans. Electr. Devi.*, vol. 63, no. 12, pp. 4825-4831, Dec. 2016.

[23] B. Subudhi and R. Pradhan, "A comparative study on maximum power point tracking techniques for photovoltaic power systems," *IEEE Trans. Sustain. Energy*, vol. 4, no. 1, pp. 89-98, Jan. 2013.

[24] A. S. Bubshait, A. Mortezaei, M. G. Simões and T. D. C. Busarello, "Power quality enhancement for a grid connected wind turbine energy system," *IEEE Trans. Ind. Appl.*, vol. 53, no. 3, pp. 2495-2505, May-June 2017.

[25] Marian P. Kazmierkowski, "Instantaneous power theory and applications to power conditioning" *IEEE Ind. Elect. Mag.*, vol. 1, no. 3, pp. 46-46, 2007.

[26] P. Tenti, H. K. M. Paredes and P. Mattavelli, "Conservative power theory, a framework to approach control and accountability issues in smart microgrids," *IEEE Trans. Pow. Elect.*, vol. 26, no. 3, pp. 664-673, March 2011.

[27] M. Barghi Latran, A. Teke and Y. Yoldaş, "Mitigation of power quality problems using distribution static synchronous compensator: a comprehensive review," *IET Pow. Elect.*, vol. 8, no. 7, pp. 1312-1328, 7 2015.

[28] B. Singh and S. R. Arya, "Adaptive theory-based improved linear sinusoidal tracer control algorithm for DSTATCOM," *IEEE Trans. Pow. Elect.*, vol. 28, no. 8, pp. 3768-3778, Aug. 2013.

[29] E. Walach and B. Widrow, "The least mean fourth (LMF) adaptive algorithm and its family," *IEEE Trans. Infor. Theo.*, vol. 30, no. 2, pp. 275-283, March 1984.
[30] L. Shi and H. Zhao, "Diffusion leaky zero attracting least mean square algorithm and its performance analysis," *IEEE Access*, 2018.
[31] S. C. Douglas, "Performance comparison of two implementations of the leaky LMS adaptive filter," *IEEE Trans. Signal Proces.*, vol. 45, no. 8, pp. 2125-2129, Aug. 1997.
[32] W. Sethares, D. Lawrence, C. Johnson and R. Bitmead, "Parameter drift in LMS adaptive filters," *IEEE Trans, Acoust., Speech, Signal Proces.*, vol. 34, no. 4, pp. 868-879, August 1986.
[33] K. Mayyas and T. Aboulnasr, "Leaky LMS algorithm: MSE analysis for Gaussian data," *IEEE Trans. Signal Proces.*, vol. 45, no. 4, pp. 927-934, April 1997.
[34] B. Singh, A. Chandra, and K. Al-Haddad, "Power quality: problems and mitigation techniques," John Wiley & Sons Ltd., United Kingdom, 2015.
[35] IEEE Recommended Practices and Requirements for Harmonic Control in Electrical Power Systems, *IEEE Standard-519*, 1992.
[36] B. Nahid-Mobarakeh, F. Meibody-Tabar and F. Sargos, "Back EMF estimation-based sensorless control of PMSM: robustness with respect to measurement errors and inverter irregularities," *IEEE Trans. Ind. Appl.*, vol. 43, no. 2, pp. 485-494, March-april 2007.
[37] M. Stiebler, "Wind Energy Systems for Electric Power Generation" Verlag Berlin Heidelberg, Springer, 2008, pp. 127-133.

Farheen Chishti (M'17) was born in Bareilly, U.P., India in 1989. She received her B.Tech degree in Electrical and Electronics Engineering from SRMSCET, Bareilly, India in 2011 and M.Tech degree (Gold Medalist) in Instrumentation and Control Engineering from Sant Longowal Institute of Engineering and Technology (S.L.I.E.T), Sangrur, Punjab, India in 2013. She is currently working towards her Ph.D. degree in the department of Electrical Engineering, Indian Institute of Technology Delhi, New Delhi, India. Her areas of research interests include, wind and solar energy generation system, energy storage, microgrid, power electronics, application of adaptive and intelligent control for power quality improvement of the distribution system, electrical machines and drives. Ms. Chishti is a recipient of IEEE-IEEMA best paper award in 2018 and recipient of second best paper award in SLIETCON-2019.

Shadab Murshid (M'15) was born in Patna, Bihar, India, in 1991. He received his B. E in Electrical Engineering from Aligarh Muslim University, Aligarh, India, in 2013. He joined Electrical Engineering Department, Indian Institute of Technology Delhi, India, for M.Tech in 2013, where he is currently working towards his Ph. D degree. His areas of interest includes electric drives, solar water pumping, wind energy conversion systems, applications of adaptive and intelligent control for renewable power generation and power quality improvement in grid interactive renewable energy systems

Bhim Singh (SM'99, F'10) was born in Rahamapur, Bijnor (UP), India, in 1956. He has received his B.E. (Electrical) from the University of Roorkee (Now IIT Roorkee), India, in 1977 and his M.Tech. (Power Apparatus & Systems) and Ph.D. from the Indian Institute of Technology Delhi, India, in 1979 and 1983, respectively. In 1983, he joined the Department of Electrical Engineering, University of Roorkee, as a Lecturer. He became a Reader there in 1988. In December 1990, he joined the Department of Electrical Engineering, IIT Delhi, India, as an Assistant Professor, where he has become an Associate Professor in 1994 and a Professor in 1997. He has been Head of the Department of Electrical Engineering at IIT Delhi from July 2014 to August 2016. Since, August 2016, he is the Dean, Academics at IIT Delhi. He is JC Bose Fellow of DST, Government of India since December 2015. He is CEA Chair Professor since January 2019. Prof. Singh has guided 79 Ph.D. dissertations, and 166 M.E./M.Tech./M.S.(R) theses. He has been filed 41 patents. He has executed more than eighty sponsored and consultancy projects. He has co-authored a text book on power quality: *Power Quality Problems and Mitigation Techniques* published by John Wiley & Sons Ltd. 2015. His areas of interest include solar PV grid interface systems, microgrids, power quality monitoring and mitigation, solar PV water pumping systems, improved power quality AC-DC converters, power electronics, electrical machines, drives and flexible alternating transmission systems.